MARTINITE, A NEW HYDRATED SODIUM CALCIUM FLUORBOROSILICATE SPECIES FROM MONT SAINT-HILAIRE, QUEBEC: DESCRIPTION, STRUCTURE DETERMINATION AND GENETIC IMPLICATIONS

Andrew M. McDonald[§]

Mineral Exploration Centre and Department of Earth Sciences, Laurentian University, Sudbury Ontario P3E 2C6, Canada

George Y. Chao[¶]

Ottawa–Carleton Geoscience Centre, Department of Earth Sciences, Carleton University, Ottawa Ontario K1S 5B6, Canada

Abstract

Martinite, ideally $(Na,\square,Ca)_{12}Ca_4(Si,S,B)_{14}B_2O_{38}(OH,Cl)_2F_2 \bullet 4H_2O$, is a new mineral species from the Poudrette quarry, Mont Saint-Hilaire, Quebec. The mineral arose through the interaction of highly fractionated, hyperagpaitic fluids with sodalite syenite xenoliths. Martinite develops both as single crystals and as rosettes of triangular to roughly hexagonal plates varying from 50 μm to a maximum of about 1 mm across. Individual crystals are typically <10 μm in thickness and dominated by {001}, and colorless to mauve to purple in color. Associated minerals include aegirine, albite, erdite, eudialyte-group minerals, galena, langite, lueshite, lovozerite-group minerals, molybdenite, posnjakite, rasvumite, sérandite, sazhinite-(Ce), sphalerite, terskite, ussingite, villiaumite, wurtzite and a number of unknown minerals, including several $Cu_{2-x}S$ minerals (UK55 group), UK53a, UK73, UK82, UK91 and a löllingite-like mineral. The mineral has a vitreous luster, is transparent, has a white streak and shows no fluorescence in either short- or long-wave ultraviolet radiation. It has a Mohs hardness of 4; the crystals are inelastic, and have a perfect cleavage on {001}. It is brittle with an uneven fracture. The calculated density is 2.51 g/cm^3. Martinite is non-pleochroic, optically biaxial (–), with α 1.529(1), β 1.549(1), γ 1.551(1) (for λ = 590 nm), $2V_{meas}$ = 38(1)°, $2V_{calc}$ = 35(1)°; no dispersion was noted. The optical orientation is $X \approx c$. On average, 19 electron-microprobe analyses gave: Na_2O 17.70, MgO 0.03, CaO 16.71, MnO 0.07, B_2O_3 (calc.) 5.02, SiO_2 48.85, TiO_2 0.06, SO_3 2.30, F 2.18, Cl 1.09 and H_2O (calc.) 4.44, O=F+Cl –1.17, total 97.28 wt.%. The empirical formula (based on 46 anions) is: $(Na_{9.19}\square_{1.99}Ca_{0.82})_{\Sigma 12}(Ca_{3.97}Mn_{0.02}Mg_{0.01})_{\Sigma 4}(Si_{13.08}S_{0.46}B_{0.45}Ti_{0.01})_{\Sigma 14.00}B_2O_{38}(OH_{1.50}Cl_{0.50})_{\Sigma 2.00}(F_{1.84}OH_{0.16})_{\Sigma 2} \bullet 4H_2O$. The principal absorption bands in the infrared spectrum include 3437, 1634 and 1011 cm^{-1} (shoulders at 1137, 1081, 898 and 862 cm^{-1}) and five bands in the region 786–498 cm^{-1}. The mineral is triclinic, space group $P\bar{1}$, a 9.5437(7), b 9.5349(6), c 14.0268(10) Å, α 108.943(1), β 74.154(1), γ 119.780(1)°, V 1038.1(1) $Å^3$, Z = 2. The strongest seven lines in the X-ray powder-diffraction pattern [d in Å(I)(hkl)] are: 13.18(100)(001), 6.58(43)(002), 2.968(37)(1$\bar{3}$0), 3.29(34)(004,$\bar{2}$20), 2.908(27)(3$\bar{2}$3), 3.02(17)($\bar{2}$11), 2.800(17)($\bar{2}$12). The structure of martinite has been refined to R = 6.30, wR^2 = 13.82%. The mineral is strongly layered, with sheets of tetrahedra (*T*), octahedra (*O*) and interlayer cations (*X*). The *T* layers are composed of six-membered rings of SiO_4 tetrahedra linked by $[(Si,B)]O_4$ and (BO_4) tetrahedra. The sheets of octahedra are composed of edge-sharing $M\phi_6$ octahedra (*M*: Na,Ca; ϕ: unspecified ligand) arranged in a closest-packed arrangement. The *O* sheets are effectively sandwiched between two symmetrically equivalent *T* layers (T_2, $\bar{T}_2$), producing a strongly bonded *T–O–T* unit. The interlayer component (*X*) houses poorly ordered Na polyhedra and H_2O molecules. Stacking of these principal components perpendicular to [001] results in a OT_2XT_2O module. Martinite is a member of the reyerite–gyrolite group. It represents the first B-bearing mineral of the group and the first mineral known to possess the $OT_2X\bar{T}_2O$ module. The name honors Robert François Martin (b. 1941), Professor of Geology at McGill University and long-time editor of *The Canadian Mineralogist*.

Keywords: martinite, new mineral species, layered borosilicate, reyerite–gyrolite group, crystal structure, Mont Saint-Hilaire, Quebec, Canada.

Sommaire

La martinite, de composition idéale $(Na,\square,Ca)_{12}Ca_4(Si,S,B)_{14}B_2O_{38}(OH,Cl)_2F_2 \bullet 4H_2O$, est une nouvelle espèce minérale découverte à la carrière Poudrette, au mont Saint-Hilaire, Québec. Ce minéral s'est formé suite à l'interaction de fluides hyper-agpaïtiques fortement évolués avec des xénolithes de syénite à sodalite. La martinite se présente en monocristaux ou bien en

[§]   *E-mail address*: amcdonald@laurentian.ca
[¶]   *Present address*: 2031 Delmar Drive, Ottawa, Ontario K1H 5P6, Canada.

rosettes de cristaux triangulaires ou en plaquettes à peu près hexagonales variant de 50 μm jusqu'à environ 1 mm. Les cristaux individuels ont une épaisseur typique de moins de 10 μm, possèdent {001} comme forme dominante, et varient d'incolore à mauve ou à violette. Lui sont associés aegyrine, albite, erdite, minéraux du groupe de l'eudialyte, galène, langite, lueshite, minéraux du groupe de la lovozérite, molybdénite, posnjakite, rasvumite, sérandite, sazhinite-(Ce), sphalérite, terskite, ussingite, villiaumite, wurtzite, et plusieurs minéraux méconnus, y inclus plusieurs membres de la série $Cu_{2-x}S$ (groupe UK55), UK53a, UK73, UK82, UK91, et un minéral du groupe de la löllingite. La martinite possède un éclat vitreux et une rayure blanche, est transparente, et ne montre pas de fluorescence en lumière ultraviolette (longueur d'onde courte ou longue). La dureté de Mohs est 4, et le clivage sur {001} est parfait, et les cristaux, inélastiques. Ils sont cassants, avec fracture inégale. La densité calculée est 2.51 g/cm³. La martinite est non pléochroïque, optiquement biaxe (–), avec α 1.529(1), β 1.549(1), γ 1.551(1) (pour λ = 590 nm), $2V_{mes}$ = 38(1)°, $2V_{calc}$ = 35(1)°, sans dispersion évidente. L'orientation optique est $X \approx c$. Les dix-neuf analyses faites avec une microsonde électronique ont donné, en moyenne, Na_2O 17.70, MgO 0.03, CaO 16.71, MnO 0.07, B_2O_3 (calc.) 5.02, SiO_2 48.85, TiO_2 0.06, SO_3 2.30, F 2.18, Cl 1.09 et H_2O (calc.) 4.44, O = F+Cl –1.17, pour un total de 97.28% (poids). La formule empirique, sur une base de 46 anions, serait $(Na_{9.19}\square_{1.99}Ca_{0.82})_{\Sigma12}(Ca_{3.97}Mn_{0.02}Mg_{0.01})_{\Sigma4}(Si_{13.08}S_{0.46}B_{0.45}Ti_{0.01})_{\Sigma14.00}B_2O_{38}(OH_{1.50}Cl_{0.50})_{\Sigma2.00}$ $(F_{1.84}OH_{0.16})_{\Sigma2}\bullet4H_2O$. Parmi les bandes d'absorption du spectre infrarouge, on trouve d'abord 3437, 1634 et 1011 cm⁻¹ (épaulements à 1137, 1081, 898 and 862 cm⁻¹), et cinq bandes dans la région 786–498 cm⁻¹. Il s'agit d'un minéral triclinique, groupe spatial $P\overline{1}$, a 9.5437(7), b 9.5349(6), c 14.0268(10) Å, α 108.943(1), β 74.154(1), γ 119.780(1)°, V 1038.1(1) Å³, Z = 2. Les sept raies les plus intenses du spectre de diffraction X, méthode des poudres [d en Å(I)(hkl)] sont: 13.18(100)(001), 6.58(43)(002), 2.968(37)(1$\overline{3}$0), 3.29(34)(004,$\overline{2}$20), 2.908(27)(3$\overline{2}$3), 3.02(17)($\overline{2}$11), 2.800(17)($\overline{2}$12). Nous en avons affiné la structure jusqu'à un résidu R de 6.30%, wR^2 = 13.82%. La martinite possède une structure stratifiée, avec couches de tétraèdres (T), octaèdres (O) et des cations interfeuillets (X). Les couches T contiennent des anneaux à six membres de tétraèdres SiO_4 interconnectés par des tétraèdres $[(Si,B)]O_4$ et (BO_4). Dans les couches O, les octaèdres $M\phi_6$ (M: Na,Ca; φ: ligand non spécifié) à arêtes partagées sont agencés de façon compacte. Ces couches sont intercalées entre deux couches T symétriquement équivalentes $(T_2, \overline{T}_2)$; il en résulte une unité T–O–T à liaisons fortes. L'interstratification X contient les polyèdres Na et les molécules de H_2O faiblement ordonnées. De l'empilement de ces composantes principales perpendiculaire à [001], il résulte un module $OT_2X\overline{T}_2O$. La martinite fait partie du groupe de la réyerite–gyrolite. C'est en fait le premier minéral de ce groupe à contenir du bore et le module $OT_2X\overline{T}_2O$. Le nom choisi honore Robert François Martin (né en 1941), professeur de géologie à l'université McGill, et rédacteur en chef de la revue The Canadian Mineralogist de longue date.

(Traduit par la Rédaction)

INTRODUCTION

Martinite, ideally $(Na,\square,Ca)_{12}Ca_4(Si,S,B)_{14}B_2O_{38}$ $(OH,Cl)_2F_2\bullet4H_2O$, is a new mineral species and member of the reyerite–gyrolite group, discovered in sodalite syenite xenoliths (SSX) at the Poudrette Quarry, Mont Saint-Hilaire, Rouville County, Quebec. It was first encountered in 1991 as a thin, hexagonal plate found in a sample submitted by M. Gilles Haineault to one of us (GYC) for identification. The mineral macroscopically resembles a colorless mica, but was found to give a distinct X-ray powder pattern that did not match any known one. In light of this finding, the mineral was considered as a potentially new species and was temporarily assigned the label UK92. It has been named martinite after Robert François Martin (b. 1941), Professor of Geology at McGill University (Montreal, Quebec, Canada) and long-time editor of The Canadian Mineralogist, in recognition for his dedication to the discipline of mineralogy (most notably his contributions to feldspars and borosilicates) and the petrology of alkaline intrusions. Both the mineral and mineral name were approved by the Commission on New Minerals and Mineral Names, IMA (IMA 2001–059). The holotype material is housed in the collection of the Canadian Museum of Nature, Aylmer, Quebec, Canada (catalogue number CMNMC 83719).

OCCURRENCE

Martinite was first encountered in September, 1991 in sodalite syenite xenoliths (SSX) from the sixth bench in the extreme southern part of the Poudrette quarry, Mont Saint-Hilaire, Rouville County, Quebec, Canada. The material used to completely characterize the species in this study was obtained from two proximal xenoliths found in situ, one discovered by M. Gilles Haineault and the other by Dr. Peter Tarassoff and Mr. Laszló Horváth. To the authors' knowledge, martinite has not been found in any SSX subsequently exposed in the quarry, nor in any of the other geological micro-environments at Mont Saint-Hilaire. The particular xenolith found by Haineault is estimated to be 30 cm across, and that by Tarassoff and Horváth, approximately 1 m in diameter. Sodalite syenite xenoliths consist predominantly of coarse-grained sodalite with lesser amounts of analcime and microcline with rare and unusual "secondary" minerals like martinite, occurring in small cavities (typically <1 cm). P. Tarassoff (pers. commun.) notes that the dominant mineralogy of the xenolith examined

by Horváth and Tarassoff is similar to that from which the species nalipoite was first described (Chao & Ercit 1991), *i.e.,* 75 modal % sodalite, 15% analcime and 10% microcline. Martinite is clearly a rare species, although the xenolith discovered by Haineault yielded approximately three dozen crystals, all in small cavities ranging in size from 0.2 to 0.5 cm. Associated minerals include aegirine, albite, erdite, eudialyte-group minerals, galena, langite, lueshite, lovozerite-group minerals, molybdenite, posnjakite, rasvumite, sérandite, sazhinite-(Ce), sphalerite, terskite, ussingite, villiaumite, wurtzite and a number of unknown minerals, including several $Cu_{2-x}S$ minerals (UK55 group), UK53a, UK73, UK82, UK91, and a löllingite-like mineral.

ORIGIN

A large number (>110) of late-stage, rare minerals (*e.g.*, ussingite, vuonnemeite, rasvumite) have been discovered in SSX at Mont Saint-Hilaire (Horváth & Pfenninger 2000), including several new to science [*e.g.*, abenakiite-(Ce), rouvilleite, lukechangite-(Ce)]. Most are characteristically enriched in alkalis and alkaline earths, are silica-poor, hydrous, and in many cases contain essential Ti, Zr, Nb, REE and F. Many are unstable under normal conditions of humidity, either decrepitating [*e.g.*, thomasclarkeite-(Y); Grice & Gault 1998] or being converted to a white efflorescence when exposed to air (*e.g.*, thermonatrite, revdite). In fact, the minerals and mineral assemblages found in the SSX very closely resemble those found in the hyperagpaitic pegmatites and hydrothermally affected rocks found in the Khibina and Lovozero massifs (Horváth & Pfenninger 2000). In view of the fact that the rare and unusual minerals in the SSX at Mont Saint-Hilaire typically occur in cavities between coarse-grained crystals of sodalite, and given their unusual chemical signatures, we contend that they are late-stage products arising through the interaction of highly evolved hyperagpaitic fluids and sodalite syenite xenoliths. The chemical composition and occurrence of martinite are consistent with its crystallization from such a fluid under similar conditions.

Most of the SSX found at Mont Saint-Hilaire have been found in a 30 m^2 area in the southeast portion of the Poudrette quarry over the period 1983–1991. However, the bulk of the unusual minerals found in such rocks were discovered in the late 1980s from a portion of this area measuring approximately 3 m^2. This area, commonly referred to as the "corner rock", was found to be very rich in SSX, most of which were positioned quite close to a large block of biotite – muscovite – quartz hornfels. Given the low porosity and dense nature of the block of hornfels, it could have acted as a cap, trapping late-stage, hyperalkaline fluids, inhibiting the release of volatiles and facilitating both the crystallization and stabilization of a large number of unusual minerals (Van Velthuizen 1990). As many of

the rare minerals found associated with martinite were also noted in SSX from the 1980s find and because the xenolith in which martinite occurs is proximal to this area, the implication is that martinite crystallized from a hyperagpaitic fluid similar to that which produced the minerals found in the 1980s discovery.

PHYSICAL AND OPTICAL PROPERTIES

Crystals of martinite develop as thin, subhedral to euhedral plates, typically measuring <10 μm in thickness and varying from 50 μm to maximum of about 1 mm across (Fig. 1). The crystals, dominated by {001}, are colorless to mauve to purple in color (those with a pinkish hue are most commonly associated with erdite). They develop both as single crystals and as rosettes of triangular to roughly hexagonal plates. No twinning was observed by optical microscopy or by single-crystal X-ray-diffraction methods. The mineral has a vitreous luster, a white streak, is transparent, and shows no fluorescence in either short- or long-wave ultraviolet radiation. It has a Mohs hardness of 4 and a perfect {001} cleavage. It is brittle with an uneven fracture. Cleavage fragments are quite inelastic, a characteristic
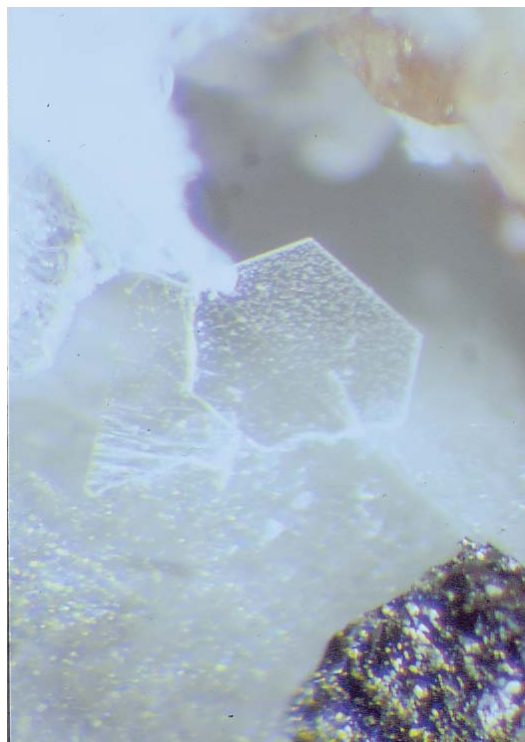

FIG. 1. A colorless, pseudohexagonal plate of martinite associated with sodalite and a clinoamphibole. The crystal is approximately 40 μm across.

useful in distinguishing martinite from similar-looking colorless micas. The density could not be determined owing to a dearth of material. The calculated density is 2.51 g/cm^3, determined using the empirical chemical formula and the unit-cell parameters derived from the crystal-structure analysis.

Martinite is non-pleochroic, biaxial negative, with α 1.529(1), β 1.549(1), γ 1.551(1) (for λ = 590 nm), $2V_{meas}$ = 38(1)°, $2V_{calc}$ = 35(1)°; no dispersion was noted. The optical orientation is $X \approx c$. A Gladstone–Dale calculation gave a compatibility index of –0.031, which is classed as excellent (Mandarino 1981).

Chemical Composition

Chemical analyses were conducted on a CAMEBAX SX50 electron microprobe using an operating voltage of 15 kV, a beam current of 10 nA and a beam diameter of approximately 10 μm. Energy-dispersion spectra (EDS) were collected using the following standards: wollastonite (Ca$K\alpha$), synthetic MnTiO$_3$ (Mn$K\alpha$, Ti$K\alpha$), periclase (Mg$K\alpha$) and celestine (S$K\alpha$). In addition, wavelength-dispersion data were collected using tugtupite (Na$K\alpha$, Si$K\alpha$, Cl$K\alpha$, F$K\alpha$) as a standard. No other elements were indicated by qualitative EDS scans. Also sought, but not detected, were Al, K, Fe and P. Nineteen analyses of five crystals gave as an average (range): Na$_2$O 17.70 (17.30–17.97), MgO 0.03 (n.d.–0.13), CaO 16.71 (15.42–17.24), MnO 0.07 (n.d.–0.16), B$_2$O$_3$ (calc.) 5.02, SiO$_2$ 48.85 (47.46–50.51), TiO$_2$ 0.06 (n.d.–0.31), SO$_3$ 2.30 (1.36–2.77), F 2.18 (1.79–2.41), Cl 1.09 (0.77–2.00) and H$_2$O (calc.) 4.44, O=F+Cl –1.17, total 97.28 wt.%. The presence of H$_2$O was confirmed by infrared spectroscopy (see below) and results of the crystal-structure analysis. Boron was also initially identified on the basis of results of

the crystal-structure analysis, and its presence was subsequently confirmed by qualitative wavelength-dispersion scans. The empirical formula, based on 46 anions, is: (Na$_{9.19}$□$_{1.99}$Ca$_{0.82}$)$_{\Sigma12}$ (Ca$_{3.97}$Mn$_{0.02}$Mg$_{0.01}$)$_{\Sigma4}$ (Si$_{13.08}$S$_{0.46}$B$_{0.45}$Ti$_{0.01}$)$_{\Sigma14.00}$ B$_2$O$_{38}$ (OH$_{1.50}$Cl$_{0.50}$)$_{\Sigma2.00}$ (F$_{1.84}$OH$_{0.16}$)$_{\Sigma2}$•4H$_2$O or, ideally, (Na,□,Ca)$_{12}$Ca$_4$ (Si,S,B)$_{14}$O$_{38}$(OH,Cl)$_2$F$_2$•4H$_2$O. The mineral does not effervesce in 1:1 HCl at room temperature.

Infrared Analysis

The infrared spectrum of martinite (Fig. 2) was obtained using a Bomem Michelson MB–120 Fourier-transform infrared spectrometer equipped with a mercury–cadmium telluride (MCT) detector. A single crystal of material was mounted in a Spectra-Tech low-pressure diamond-anvil microsample cell. The spectrum, a sum total of 200 co-added scans, was obtained over the range 4000–400 cm^{-1}. Absorption bands were identified using the data of Farmer (1974). The spectrum shows a broad band centered at the 3437 cm^{-1} region (O–H stretching), and a relatively weak, broad band at 1634 cm^{-1} (H–O–H bending). The spectrum also shows a strong, sharp band at 1011 cm^{-1}, with shoulders at 1137, 1081, 898 and 862 cm^{-1} (asymmetric O–Si–O, O–B–O stretching) and five sharp, weak to moderately strong bands in the region 786–498 cm^{-1} (symmetric Si–O–Si, O–B–O stretching; Farmer 1974). As the ranges in the frequency modes for BO$_4$ and SiO$_4$ tetrahedra overlap [asymmetric stretching: 1100–850 cm^{-1} for BO$_4$ *versus* 1200–900 cm^{-1} for SiO$_4$; symmetric stretching: 850–700 cm^{-1} for BO$_4$ *versus* 800–400 cm^{-1} for SiO$_4$; Farmer (1974)], it is not possible to unequivocally assign absorption bands in these regions.

X-Ray Crystallography and Crystal-Structure Determination

X-ray powder-diffraction data (Table 1) were collected with a Debye–Scherrer camera 114.6 mm in diameter employing Ni-filtered Cu$K\alpha$ radiation (λ = 1.5418 Å). Interplanar spacing and intensity data were determined using a scanned X-ray film. Whether or not an *hkl* plane contributed to a reflection was determined from the powder pattern calculated using the atom parameters determined in the crystal-structure analysis and the program POWDERCELL (Nolze & Kraus 1998).

A single crystal mounted approximately parallel to c^* was used for the collection of X-ray intensity data. These were collected on a fully automated Enraf–Nonius CAD4 four-circle diffractometer operated at 50 kV, 26 mA, with graphite-monochromated Mo$K\alpha$ radiation. It should be noted that the unit cell given herein has been transformed from that originally referenced (IMA #2001–059, so as to adhere to the IUCr convention, $c < a < b$), in order to emphasize the relationship between martinite and minerals of the reyerite group. A full sphere of X-ray intensity data out to 2θ = 56.7°
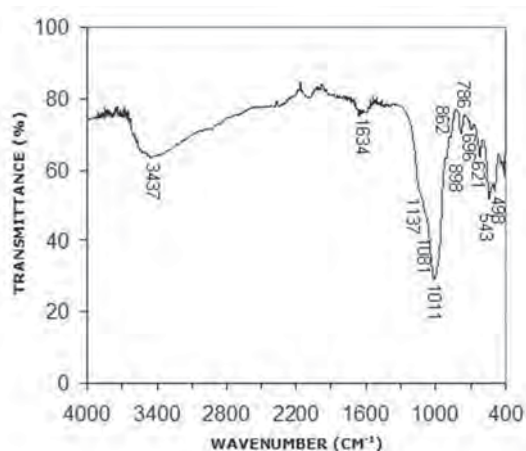

FIG. 2.   Infrared spectrum of martinite.

was collected using a θ:2θ scan-mode, with scan speeds inversely proportional to intensity. With these operating conditions, no decrepitation was evident in the final analysis of the reflections used as intensity standards. Data measurement and reduction (Lorentz, polarization, background, scaling) were carried out using the NRCVAX set of computer programs (Gabe *et al*. 1989). No absorption correction was applied to the data, given the low μ value for the mineral. Information pertinent to the data collection and structure determination is provided in Table 2.

Solution and refinement of the crystal structure were accomplished using the SHELX–93 package of programs (Sheldrick 1993). The crystal structure was solved using direct methods, with scattering curves and anomalous dispersion coefficients taken from Cromer & Mann (1968) and Cromer & Liberman (1970), respectively. Preliminary X-ray precession photographs indicated P^* diffraction symmetry. Phasing of a set of normalized structure-factors gave a mean value of $|E^2 - 1|$ equal to 0.972 (predicted values: 0.968, centrosymmetric, 0.736, non-centrosymmetric); on this basis, $P\bar{1}$ was selected, and proved to be the correct space-group. Phase-normalized factors were calculated and used to produce an E-map on which were located Ca, along with several Si and O sites. The remaining Na and O sites were located on subsequent Fourier-difference maps. Results from this model indicated one of the

tetrahedrally coordinated sites [$B(1)$] to have excessively short Si–O bond distances in the range 1.45–1.50 Å, and the other to have relatively short Si–O bond distances of 1.50–1.58 Å [$Si(7)$]. Refinement of the electron scattering (assuming Si) in the first site gave 4.9(1) electrons and for the second, 9.7(1) electrons. In light of this finding, a qualitative wavelength-dispersion scan was made, which confirmed the presence of B in the mineral. On the basis of these data, the B has been assigned to one site, and a mixed (Si,B) occupancy to the other. Determination of those O sites likely occupied by OH or H_2O was made on the basis of bond-valence calculations in conjunction with charge-balance considerations. Anisotropic refinement of this model indicated that the $Na2$, $Na3$, $Na6$ and $Ca2$ sites have lower-than-ideal site-occupancy factors (SOF; Table 3). Attempts at refining the $Na2$, $Na3$ and $Na6$ sites with mixed (Na,Ca) occupancies were not successful, and the assumption was thus made that these sites are partially vacant. In the case of $Na6$, further refinement suggested pronounced elongation in the [001] direction, and the site was subsequently split into two partially occupied sites ($Na6a$, $Na6b$). In the case of the $Ca2$ site, the refinement was conducted assuming a mixed (Ca,Na) occupancy. Final least-squares refinement of this model gave residuals of $R = 6.30$ and $wR^2 = 13.82\%$, with maximum and minimum electron-densities of +2.54 and –0.94 e/Å^3.

Table 3 contains the final positional and displacement parameters, with selected interatomic distances in Table 4, and bond-valence sums in Table 5. Observed and calculated structure-factors are available at the Depository of Unpublished Data on the MAC web site [document Martinite CM45_xxx].

CRYSTAL-STRUCTURE DESCRIPTION

Martinite is strongly layered perpendicular to [001]; it consists of sheets of tetrahedra (T), octahedra (O) and

TABLE 1. MARTINITE: X-RAY POWDER-DIFFRACTION DATA

I meas	I calc	d obs	d calc	hkl	I meas	I calc	d obs	d calc	hkl
100	100	13.18	13.144	001	5	1	2.135	2.146	$3\bar{4}0$
43	43	6.58	6.572	002	2	3	1.993	1.998	$2\bar{1}5$
10	1	4.81	4.819	$\bar{1}20$	5	1	1.931	1.939	$2\bar{1}7$
7	1	3.89	3.888	$\bar{1}21$		2		1.936	$\bar{1}34$
4	2	3.53	3.529	013	5	1	1.771	1.774	$\bar{1}43$
5	3	3.45	3.408	$\bar{2}21$		1		1.774	$4\bar{5}4$
34	23	3.29	3.286	004	5	1	1.728	1.730	$\bar{1}35$
	6		3.285	$\bar{2}20$	5	1	1.684	1.688	$3\bar{1}5$
5	2	3.21	3.222	202		1		1.686	$0\bar{1}8$
11	3	3.09	3.090	$2\bar{3}1$		1		1.678	$3\bar{2}8$
	3		3.087	$2\bar{2}4$	5	1	1.624	1.626	$\bar{2}44$
17	12	3.02	3.036	$2\bar{1}1$		1		1.626	$\bar{2}70$
37	21	2.968	2.979	$1\bar{3}0$		1		1.622	217
27	21	2.908	2.916	$3\bar{2}3$	5	1	1.599	1.605	$\bar{4}51$
17	17	2.800	2.810	$2\bar{1}2$		1		1.599	$\bar{2}17$
15	10	2.729	2.734	$\bar{1}13$	5	1	1.552	1.558	421
8	7	2.647	2.654	$3\bar{2}4$		1		1.556	229
6	4	2.563	2.568	213		1		1.554	$6\bar{4}2$
5	2	2.436	2.431	$\bar{3}22$		1		1.553	$4\bar{5}7$
2	3	2.374	2.380	$4\bar{2}2$		1		1.550	$3\bar{1}6$
4	2	2.347	2.353	$1\bar{3}5$	5	1	1.522	1.529	422
	2		2.352	$2\bar{4}1$		1		1.527	$6\bar{4}1$
5	1	2.284	2.289	$1\bar{4}2$		1		1.520	$\bar{4}05$
	1		2.288	$3\bar{4}2$	5	2	1.502	1.504	$2\bar{6}5$
	1		2.286	214		2		1.502	$1\bar{3}9$
5	1	2.240	2.252	115	5	2	1.4650	1.4646	218
	2		2.249	$\bar{2}14$	5	1	1.4375	1.4326	$\bar{2}61$
2	1	2.191	2.191	006	5	1	1.3989	1.3998	$\bar{3}27$
3	3	2.175	2.178	$\bar{1}33$	5	1	1.3182	1.3179	$2\bar{6}8$
5	1	2.156	2.155	$\bar{1}33$					

The d values are expressed in Å.

TABLE 2. MISCELLANEOUS INFORMATION FOR MARTINITE

Space group	$P\bar{1}$	Diffractometer	Enraf Nonius CAD4
a (Å)	9.5437(7)	Radiation	Mo$K\alpha$ (50 kV, 26 mA)
b	9.5349(6)	Monochromator	Graphite
c	14.0268(10)	Crystal shape	Plate flattened on [001]
α (°)	108.943(1)	Crystal size	0.04 × 0.12 × 0.12 mm
β	74.154(1)	μ(Mo$K\alpha$)	2.08 mm^{-1}
γ	119.780(1)	Z	2
V (Å^3)	1038.1(1)		

Chemical formula	$(Na,\square,Ca)_{12}Ca_4(Si,S,B)_{14}B_2O_{38}(OH,Cl)_2F_2 \cdot 4H_2O$
Intensity-data collection	θ:2θ scan mode
2θ limit	57°
Number of unique reflections	4828
Number of observed reflections	4241
Criterion for observed reflections	$F_o > 4\sigma(F_o)$
GoOF	1.139
Final R for all observed reflections (%)	6.30
Final wR^2 for all observed reflections (%)	13.82

The unit-cell parameters were refined from four-circle diffractometer data.

TABLE 3. POSITIONAL AND DISPLACEMENT PARAMETERS FOR MARTINITE

	x	y	z	SOF	U_{11}	U_{22}	U_{33}	U_{23}	U_{13}	U_{12}	U_{eq}
Na1	1/2	1/2	1/2	1.00	0.013(1)	0.010(1)	0.017(1)	0.003(1)	-0.003(1)	0.006(1)	0.0128(5)
Na2	0.1472(4)	0.9626(5)	0.9138(2)	0.86(1)	0.030(2)	0.057(3)	0.027(2)	0.002(1)	-0.006(1)	-0.014(2)	0.055(2)
Na3	0.3646(5)	0.1039(7)	0.0907(3)	0.81(1)	0.044(2)	0.143(5)	0.027(2)	0.030(2)	0.012(2)	0.064(3)	0.062(2)
Na4	0.7988(3)	0.5957(3)	0.2424(2)	1.00	0.021(1)	0.019(1)	0.035(1)	0.0073(9)	-0.0064(9)	0.0071(9)	0.0247(5)
Na5	0.2217(2)	0.0794(2)	0.4938(1)	0.51(1)	0.0123(8)	0.0095(7)	0.0192(8)	0.0033(5)	-0.0038(5)	0.0039(5)	0.0137(5)
Ca				0.49(1)							
Na6a	0.5980(13)	0.4280(12)	0.9084(9)	0.34(2)	0.065(7)	0.029(5)	0.022(6)	0.004(4)	0.002(4)	0.027(4)	0.039(4)
Na6b	0.5993(16)	0.4843(15)	0.9772(15)	0.45(2)	0.120(10)	0.052(7)	0.106(16)	0.003(8)	-0.041(8)	0.014(6)	0.095(6)
Ca1	0.9210(1)	0.6498(1)	0.51495(7)	1.00	0.0098(4)	0.0082(4)	0.0174(5)	0.0028(4)	-0.0023(3)	0.0023(4)	0.0125(2)
Ca2	0.3542(1)	0.7881(1)	0.49742(8)	0.80(1)	0.0086(6)	0.0101(6)	0.0170(6)	0.0046(4)	0.0019(4)	0.0031(4)	0.0120(4)
Na				0.20(1)							
Si1	0.4544(2)	0.7607(2)	0.7078(1)	1.00	0.0087(6)	0.0095(6)	0.0174(6)	0.0035(5)	-0.0031(5)	0.0041(5)	0.0114(3)
Si2	0.5898(2)	0.5189(2)	0.7142(1)	1.00	0.0095(6)	0.0073(6)	0.0161(6)	0.0034(5)	-0.0025(5)	0.0027(5)	0.0111(3)
Si3	0.9664(2)	0.0103(2)	0.7118(2)	1.00	0.0093(6)	0.0078(6)	0.0184(7)	0.0039(5)	-0.0032(5)	0.0020(5)	0.0121(3)
Si4	0.6572(2)	0.8555(2)	0.2880(1)	1.00	0.0087(6)	0.0072(6)	0.0173(6)	0.0041(5)	-0.0026(5)	0.0016(5)	0.0114(3)
Si5	0.1576(2)	0.7450(2)	0.2969(1)	1.00	0.0090(6)	0.0075(6)	0.0186(7)	0.0037(5)	-0.0031(5)	0.0026(5)	0.0117(3)
Si6	0.0822(2)	0.6296(2)	0.7061(1)	1.00	0.0087(6)	0.0068(6)	0.0167(6)	0.0037(5)	-0.0024(5)	0.0018(5)	0.0111(3)
Si7	0.5249(2)	0.1030(2)	0.8299(2)	0.58(1)	0.0074(10)	0.0073(10)	0.0201(11)	0.0056(7)	-0.0026(7)	0.0019(7)	0.0114(6)
B				0.42(1)							
B	0.8556(6)	0.7646(6)	0.8274(5)	1.00	0.008(3)	0.006(3)	0.029(3)	0.006(2)	-0.001(2)	0.003(2)	0.014(2)
F	0.7650(4)	0.6226(4)	0.4225(2)	1.00	0.024(2)	0.021(2)	0.022(2)	0.003(1)	-0.005(1)	0.009(1)	0.0225(7)
O1	0.0998(4)	0.6189(5)	0.5878(3)	1.00	0.013(2)	0.021(2)	0.019(2)	0.009(2)	-0.002(1)	0.003(1)	0.0187(8)
O2	0.1730(5)	0.8013(4)	0.4153(3)	1.00	0.020(2)	0.016(2)	0.021(2)	0.001(1)	-0.007(1)	0.008(2)	0.0190(8)
O3	0.3896(4)	0.0674(4)	0.5969(3)	1.00	0.018(2)	0.014(2)	0.016(2)	0.002(1)	-0.001(1)	0.004(1)	0.0183(8)
O4	0.6748(5)	0.4869(3)	0.6005(5)	1.00	0.021(2)	0.019(2)	0.019(2)	0.004(2)	0.003(2)	0.006(2)	0.0228(8)
O5	0.5120(4)	0.7745(5)	0.5929(3)	1.00	0.017(2)	0.025(2)	0.021(2)	0.008(2)	-0.002(1)	0.009(2)	0.0202(8)
O6	0.9588(6)	0.9167(5)	0.5956(3)	1.00	0.047(3)	0.024(2)	0.025(2)	-0.004(2)	-0.015(2)	0.022(2)	0.030(1)
O7	0.7419(4)	0.3085(4)	0.2590(3)	1.00	0.010(2)	0.016(2)	0.024(2)	0.003(1)	-0.004(1)	0.006(1)	0.0163(7)
O8	0.5580(4)	0.6530(4)	0.2563(3)	1.00	0.014(2)	0.010(2)	0.024(2)	0.006(1)	-0.006(1)	0.002(1)	0.0160(7)
O9	0.3664(4)	0.0743(4)	0.7955(3)	1.00	0.014(2)	0.016(2)	0.028(2)	0.013(1)	-0.005(1)	0.003(1)	0.0182(8)
O10	0.0089(4)	0.7533(4)	0.7795(3)	1.00	0.012(2)	0.011(2)	0.037(2)	0.003(2)	-0.003(2)	0.005(1)	0.0205(8)
O11	0.1531(4)	0.1118(4)	0.7390(3)	1.00	0.007(2)	0.015(2)	0.033(2)	0.008(2)	-0.003(1)	0.002(1)	0.0191(8)
O12	0.4926(4)	0.6294(4)	0.7335(3)	1.00	0.013(2)	0.011(2)	0.033(2)	0.007(1)	-0.005(1)	0.006(1)	0.0180(7)
O13	0.0885(4)	0.8430(4)	0.2608(3)	1.00	0.014(2)	0.012(2)	0.027(2)	0.008(1)	-0.003(1)	0.006(1)	0.0167(7)
O14	0.8529(4)	0.8952(5)	0.7917(3)	1.00	0.014(2)	0.018(2)	0.045(2)	0.022(2)	0.006(2)	0.006(2)	0.0241(9)
O15	0.7101(4)	0.6048(4)	0.8007(3)	1.00	0.014(2)	0.009(2)	0.025(2)	0.007(1)	-0.009(1)	-0.002(1)	0.0168(7)
O16	0.0249(4)	0.5524(4)	0.2668(3)	1.00	0.014(2)	0.009(2)	0.031(2)	0.008(1)	-0.004(2)	0.002(1)	0.0181(5)
O17	0.3281(4)	0.7646(4)	0.2255(3)	1.00	0.011(2)	0.014(2)	0.035(2)	0.010(2)	0.004(1)	0.006(1)	0.0202(8)
O18	0.5368(4)	0.9332(4)	0.7906(3)	1.00	0.013(2)	0.011(2)	0.033(2)	0.000(2)	-0.010(2)	0.005(1)	0.0192(8)
O19	0.5210(6)	0.1595(6)	0.9436(4)	1.00	0.042(3)	0.032(2)	0.036(2)	0.019(2)	-0.002(2)	0.020(2)	0.034(1)
OH20	0.8492(5)	0.8198(6)	0.9379(3)	1.00	0.027(2)	0.027(2)	0.028(2)	-0.001(2)	-0.005(2)	0.004(2)	0.032(1)
OW21	0.8416(10)	0.5423(9)	0.0441(6)	1.00	0.096(6)	0.059(5)	0.081(6)	0.031(4)	0.036(4)	0.043(4)	0.082(2)
OW22	0.1918(10)	0.8225(10)	0.0038(6)	1.00	0.082(6)	0.070(5)	0.102(7)	0.022(4)	0.016(5)	0.043(5)	0.086(4)

interlayer cations (X). The S layers (S for silicate) are composed of six-membered, pseudohexagonal rings of SiO$_4$ tetrahedra that are linked by [(Si,B)]O$_4$ and (BO$_4$) tetrahedra (Fig. 3) to complete the sheet. The apices of the SiO$_4$ tetrahedra in these rings all point in a common direction toward the O sheet ([001]), but deviate slightly away from [001] owing to geometrical restrictions resulting from linkages made with overlying O sheets. This deviation contributes to a reduction in the overall symmetry of the mineral, although a strong pseudohexagonal character is retained. In general terms, the Si–O bond distances involving oxygen atoms in the plane of these rings (*i.e.*, the a–b plane) are rather normal (~1.61–1.64 Å), whereas those involving apical atoms (~1.61–1.64 Å), whereas those involving apical atoms of oxygen ($O1 \rightarrow O6$, corresponding to bridging atoms of oxygen that link to O sheets) are noticeably shorter (1.58–1.60 Å). The (Si,B)O$_4$ and BO$_3$(OH) tetrahedra that interconnect the pseudohexagonal silicate rings in

the *a–b* plane are oriented such that their apices point away from the *O* sheets, toward the interlayer region of the structure. Neither of these bridging tetrahedra directly link to like tetrahedra in adjacent *T* sheets [along (001)], a feature consistent with that in related minerals (*e.g.*, fedorite; Mitchell & Burns 2001). The sheets of tetrahedra in martinite resemble the double sheets of SiO_4 and AlO_4 tetrahedra observed in minerals like reyerite and gyrolite. These are referred to as S_2 sheets by Merlino (1988a, b), which differ in shape and possible condensation relative to those referred to as S_1 sheets. The designation of sheets of tetrahedra using the symbol *S* is most unfortunate, as *T* is considerably more

accurate (they represent sheets of tetrahedra) and avoids unnecessary confusion (*e.g.*, S is present in the sheets of tetrahedra found in martinite). Thus, whereas there may be other examples describing the crystal structures of related phases using the *S* notation to represent sheets of tetrahedra present in the literature, we have chosen to refer to such sheets using the term *T*. Thus, in martinite, the sheets of tetrahedra present are T_2 sheets.

Four distinct cations (*Na*1 in a special position at the inversion center, *Na*5, *Ca*1 and *Ca*2 in general positions) occur in the sheets of octahedra (*O*). The *O* sheets consist of a closest-packed arrangement of seven edge-sharing $M\phi_6$ octahedra (*M* = Na,Ca; φ: unspecified ligand) (Fig. 4). These sheets are joined to the T_2 layers through apical atoms of oxygen from the SiO_4 tetrahedra of the pseudohexagonal rings (Fig. 5). The *O* sheets are effectively sandwiched between two symmetrically equivalent T_2 layers ($T_1\overline{T}_2$), producing a strongly bonded *T–O–T* unit (Fig. 6). The $(Si,B)O_4$ and $BO_3(OH)$ tetrahedra (*i.e.*, those tetrahedra not part of the six-membered rings of SiO_4 tetrahedra) have their apical directions oriented along [001], away from the *T–O–T* unit and toward an interlayer component (*X*) that houses poorly ordered Na polyhedra and H_2O molecules. The bonding between polyhedra in the *X* component and the adjacent T_2 sheets is weak, and likely involves considerable H-bonding (although the intensity data were not of sufficient resolution to discern H positions). For example, the apex of the $BO_3(OH)$ tetrahedron, [OH20], corresponds to (OH); for the $(Si,B)O_4$ tetrahedra, the lower-than-ideal bond-valence sum (1.406 *vu*; Table 5) is suggestive of significant $O^{2-} \rightleftharpoons$ (OH) disorder. In any event, weak bonding between the T_2 sheet and the *X* layer is the most plausible factor responsible for the perfect {001} cleavage observed in the mineral.

TABLE 4. SELECTED INTERATOMIC DISTANCES (Å) IN MARTINITE

|					
Na1	- F × 2	2.383 (3)	Na2	- O9	2.304 (5)
	- O5 × 2	2.476 (4)		- OW22	2.350 (9)
	- O4 × 2	2.527 (4)		- O10	2.362 (5)
<Na1	- φ>	2.462		- OH20	2.410 (5)
				- OH20'	2.445 (5)
Na3	- O19	2.239 (6)	<Na2	- O>	2.374
	- O14	2.272 (5)			
	- O18	2.315 (5)	Na4	- F	2.368 (4)
	- OW22	2.446 (9)		- O16	2.517 (4)
	- OH20	2.639 (6)		- O11	2.526 (4)
<Na3	- O>	2.382		- O12	2.546 (4)
				- O8	2.560 (4)
Na5	- F	2.312 (3)		- O7	2.591 (4)
	- O2	2.370 (4)		- O13	2.607 (4)
	- O5	2.403 (4)		- OW21	2.621 (4)
	- O6	2.411 (4)	<Na4	- φ>	2.542
	- O3	2.495 (4)			
	- O6'	2.521 (5)	Na6a	- O15	2.291 (14)
<Na5	- φ>	2.419		- O17	2.394 (10)
				- O19	2.471 (9)
Na6b	- OW21	2.462 (14)		- O8	2.782 (13)
	- O19	2.706 (12)		- OW21	2.948 (14)
	- O15	2.792 (15)	<Na6a	- O>	2.577
	- OH20	3.010 (10)			
<Na6b	- O>	2.595	Ca1	- F	2.291 (3)
				- O6	2.309 (4)
Ca2	- O5	2.344 (4)		- O4	2.328 (4)
	- O3	2.387 (4)		- O1	2.386 (4)
	- O2	2.394 (4)		- O2	2.419 (4)
	- O1	2.420 (4)		- O1'	2.436 (4)
	- O4	2.447 (4)	<Ca1	- φ>	2.362
	- O3'	2.471 (5)			
<Ca2	- O>	2.410	Si1	- O5	1.579 (4)
				- O18	1.625 (4)
Si2	- O4	1.587 (4)		- O12	1.628 (3)
	- O15	1.624 (3)		- O7	1.630 (3)
	- O8	1.634 (3)	<Si1	- O>	1.616
	- O12	1.640 (3)			
<Si2	- O>	1.621	Si3	- O6	1.585 (4)
				- O14	1.609 (4)
Si4	- O3	1.583 (4)		- O13	1.627 (3)
	- O11	1.631 (3)		- O11	1.635 (3)
	- O9	1.635 (4)	<Si(3)	- O>	1.614
	- O8	1.637 (3)			
<Si4	- O>	1.622	Si5	- O2	1.594 (4)
				- O17	1.617 (4)
Si6	- O1	1.595 (4)		- O16	1.632 (3)
	- O10	1.605 (4)		- O13	1.632 (3)
	- O16	1.630 (3)	<Si(5)	- O>	1.616
	- O7	1.638 (3)			
<Si6	- O>	1.617	Si7	- O19	1.506 (5)
				- O17	1.565 (4)
B	- OH20	1.460 (6)		- O9	1.580 (4)
	- O10	1.475 (5)		- O18	1.584 (4)
	- O15	1.483 (5)	<Si(7)	- O>	1.559
	- O14	1.499 (5)			
<B	- O>	1.479			
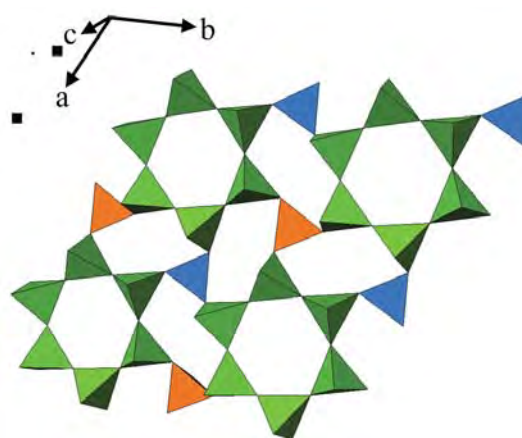
FIG. 3. A plan view of the T_2 layer of tetrahedra in martinite. The six-membered silicate rings are cross-linked by Si(7) O_4 (orange) and by $BO_3(OH)$ (blue) tetrahedra.

FIG. 4. A plan view of the closest-packed O layer in martinite. The four types of edge-sharing $M\phi_6$ octahedra are defined in terms of the central cation: $Na1$ (yellow), $Na5$ (purple), $Ca1$ (red) and $Ca2$ (orange). Green spheres represent F.
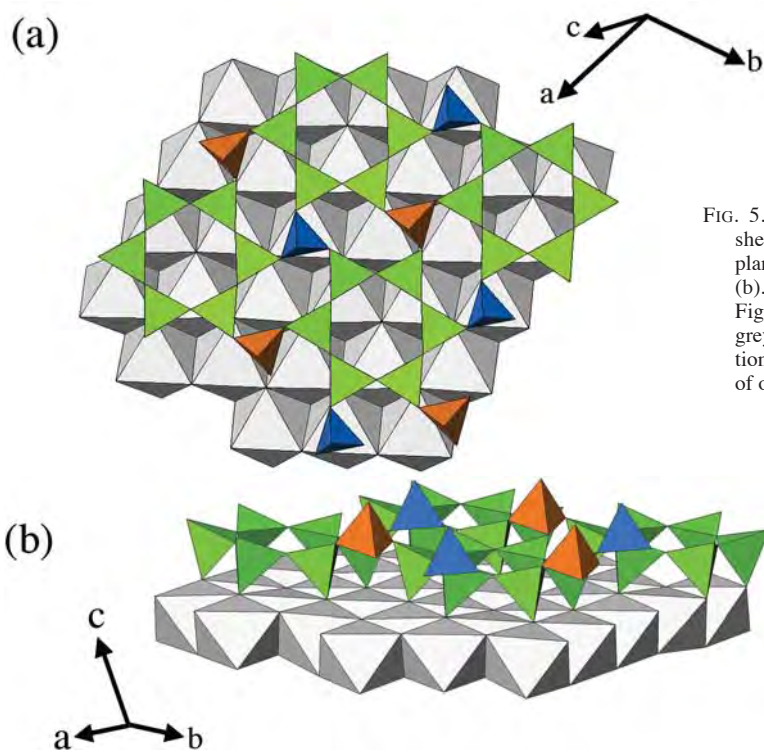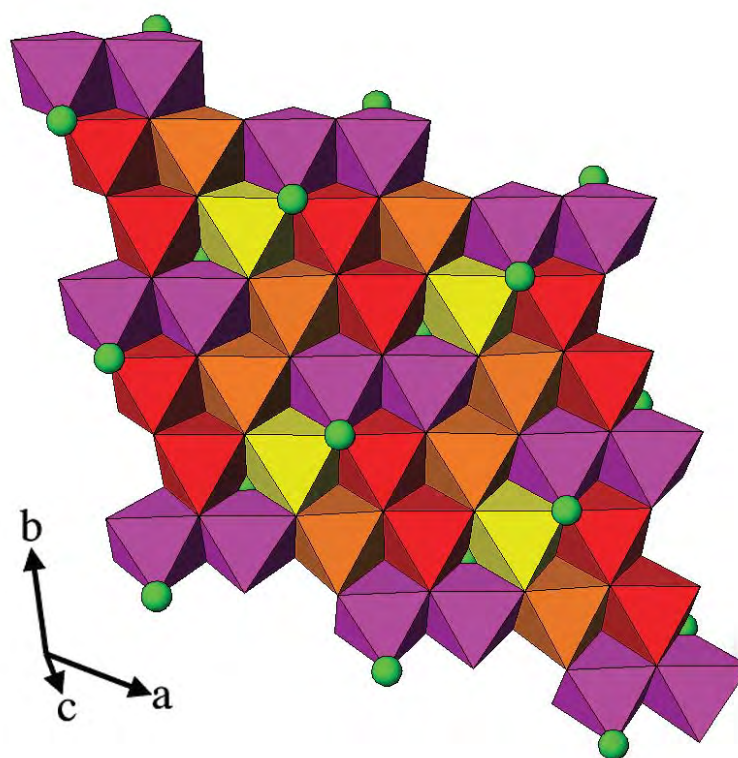

FIG. 5. Linkages between the O and T_2 sheets in martinite projected on the ab plane in (a), and inclined to this plane in (b). The legend for the tetrahedra as in Figure 3, and all the $M\phi_6$ octahedra in grey (for the sake of simplicity, no distinction is made between the individual types of octahedra).

The inelastic, brittle nature of the cleavage fragments observed in martinite (an important diagnostic feature of the mineral) can be explained by the presence of Na polyhedra of low coordination in the X layer, producing an interlayer of quasi-octahedra, similar to that found in brittle micas or in chlorite-group minerals.

RELATED PHASES

Martinite is a member of the so-called reyerite–gyrolite group (Bonaccorsi & Merlino 2005), which consists of a number of layered alkali and alkaline-earth silicate and aluminosilicate hydrates having a trigonal or strongly pseudotrigonal symmetry (Table 6). The crystal structures of these phases contain sheets of octahedra (O), tetrahedra (T), a variety of interlayer components (X), along with symmetry equivalents of all three (indicated by a "bar" $e.g.$, $\overline{O}$) using the terminology of Merlino (1988a). The sheets of octahedra are all closest packed (brucite-like), occupied either solely by Ca or by a combination of Ca, Na or Mn. Two different

sheets of tetrahedra are present in minerals belonging to this group, each with the composition T_8O_{20} (T: tetrahedrally coordinated cation, Si, Al, B or, in trace
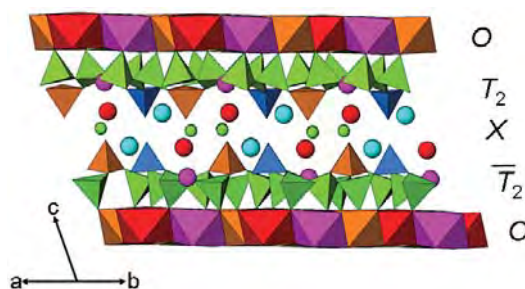
FIG. 6. The $OT_2\overline{T}_2O$ module in martinite. Legend as in Figures 3 and 4, with H_2O (green spheres), Na2 and Na6 (blue spheres), Na3 (red spheres) and Na4 (purple spheres).

TABLE 5. EMPIRICAL BOND-VALENCES (*vu*) FOR MARTINITE*

	Na1	Na2†	Na3†	Na4	Na5	Na6a†	Na6b†	Ca1	Ca2†	Si1	Si2	Si3	Si4	Si5	Si6	Si7†	B	ΣBV
F	0.148 ×2		0.154		0.226			0.297										0.973
O1								0.322 0.282	0.258						1.082			1.944
O2					0.245			0.295	0.262					1.084				1.886
O3					0.212				0.262 0.253				1.117					1.844
O4	0.140 ×2							0.377	0.255	1.105								2.017
O5	0.161 ×2				0.235				0.269	1.129								1.955
O6					0.233 0.206			0.397			1.111							1.947
O7			0.118							0.984				0.963				2.065
O8		0.128		0.023							0.973	0.965						2.089
O9		0.212										0.971					0.881	2.064
O10		0.182												1.053			0.755	1.990
O11			0.141									0.971	0.981					2.093
O12		0.035		0.133						0.989	0.958							2.115
O13			0.113									0.992	0.979					2.084
O14				0.220									1.041				0.708	1.969
O15						0.085	0.029		1.000							0.739		1.853
O16				0.144										1.005	0.984			2.133
O17						0.064								1.019		0.917		2.000
O18			0.197						0.997							0.871		2.065
O19				0.241		0.052	0.037								1.076			1.406
OH20		0.145	0.159	0.082		0.016											0.786	1.188
OW21			0.109			0.014	0.072											0.195
OW22		0.188	0.137															0.325
ΣBV	0.898	0.886	0.912	1.040	1.357	0.238	0.154	1.970	1.559	4.099	4.036	4.115	4.034	4.087	4.082	3.745	3.130	

* Parameters from Brese & O'Keeffe (1991). ‡ Calculated using the refined site-occupancy factors. BV: bond valence.

TABLE 6. CRYSTALLOGRAPHY, CHEMICAL FORMULAE AND STRUCTURAL SCHEME FOR MEMBERS
OF THE REYERITE GROUP AND RELATED SYNTHETIC PHASES

Mineral	Crystal-chemical formula	Space group	a (Å)	b (Å)	c (Å)	α (°)	β (°)	γ (°)	Structural scheme
Fedorite [1]	$(Na,K)_{2-3}(Ca,Na)_7$ $(Si,Al)_{16}O_{38}F_2 \cdot 3\text{-}4H_2O$	$P\bar{1}$	9.6450	9.6498	12.6165	102.427	96.247	119.894	$OT_2\bar{T}_2O$
K-phase [2]	$Ca_7Si_{16}O_{38}(OH)_2$	$P\bar{1}$	9.70	9.70	12.25	108.5	78.0	120.0	ibid.
Reyerite [3]	$(Na,K)_2Ca_{14}Si_{22}Al_2O_{58}(OH)_8 \cdot 6H_2O$	$P\bar{1}$	9.765		19.067				$T_1OT_2\bar{T}_2\bar{O}T_1$
Truscottite [4]	$(Ca,Mn)_{14}Si_{14}O_{58}(OH)_8 \cdot 2H_2O$	$P\bar{1}$	9.735		18.83				ibid.
Martinite [5]	$(Na,\bullet,Ca)_{12}Ca_4(Si,S,B)_{14}B_2O_{38}$ $(OH,Cl)_2F_2 \cdot 4H_2O$	$P\bar{1}$	9.5437	9.5349	14.0268	108.943	74.154	119.780	$OT_2\,X\bar{T}_2O$
Z-phase [6]	$Ca_9Si_{16}O_{40}(OH)_2 \cdot (14+x)H_2O$	?	9.65	9.65	15.3	?	?	120.0	ibid.
Gyrolite [7]	$Ca_{16}NaSi_{23}AlO_{60}(OH)_8 \cdot 14H_2O$	$P\bar{1}$	9.74	9.74	22.40	95.7	91.5	120.0	$T_1OT_2X\bar{T}_2\bar{O}\,T_1$
Tungusite [8]	$Ca_{14}Fe^{2-}{}_9Si_{24}O_{60}(OH)_{22}$	$P\bar{1}$	9.714	9.721	22.09	90.13	98.3	120.0	ibid.
Orlymanite [9]	$Ca_4Mn_3Si_8O_{20}(OH)_6 \cdot 2H_2O$	$P3$ or $P\bar{3}$	9.60		35.92				$T_1O\bar{T}_1\bar{O}T_2$ $OT_1\bar{O}T_1$ (?)

1 Mitchell & Burns (2001), 2 Gard *et al.* (1981), 3 Merlino (1988a), 4 Lachowski *et al.* (1979), 5 this study, 6 Gard *et al.* (1975),
7 Merlino (1988a), 8 Ferraris *et al.* (1995), 9 Peacor *et al.* (1990).

amounts as seen in martinite, S). The first sheet, referred to as T_1, has four tetrahedra whose vertices point in one direction and four tetrahedra with vertices pointing in the opposite direction, this sheet being connected to sheets of octahedra (O) on both sides. The second sheet, referred to as T_2, has six tetrahedra whose vertices point in one direction (toward a sheet of octahedra) and two whose vertices point in the other. All members of the reyerite–gyrolite group possess T_2 layers of tetrahedra, although only some members possess *both* T_1 and T_2 layers (*e.g.*, reyerite itself).

The T_2 layers present in phases belonging to the reyerite–gyrolite group may or may not be condensed through shared vertices along [001]. In cases where they are, as in fedorite, double layers, $T_2\bar{T}_2$, of composition $T_{16}O_{38}$, are formed. These double layers also result in the development of large channels, within which ions of large radius (K, Na) and H_2O can be accommodated. In situations where the double layers are not condensed, as in gyrolite, an interlayer component containing ions of large radius coordinated by H_2O is formed. Such interlayer components can be highly variable in terms of thickness and content (*cf.* martinite *versus* gyrolite); they also play an important role in the industrial applications of these minerals (and their related synthetic counterparts), as they are expandable and in some cases, the expansion is reversible (*e.g.*, gyrolite; Garbev *et al.* 2004).

Articulation between the O and T layers is distinctly complicated by the fact that large-radius ions, typically Ca, occupy the O layers. This leads to significant misfit in the T layer as it attempts to link to the O layer. In turn, the misfit results in a lowering of the sheet symmetry from hexagonal or trigonal to triclinic. As discussed by Guggenheim & Eggleton (1987), this type of misfit involving tetrahedra is compensated by modulation or "periodic perturbation" of the sheet, involving reversals in the apical directions of tetrahedra, rotation of individual tetrahedra about an axis normal to the layers, and relative rotation of the sheets of tetrahedra and octahedra about a crystallographic axis (typically **c**). As is seen in Figure 5, all three of these mechanisms are in operation.

The T, O and X structural components in reyerite-group minerals are arranged in a variety of ways to create modules that are stacked perpendicular to [001]; in this regard, they possess crystal structures reminiscent of those found in typical phyllosilicates. For example, the crystal structure of reyerite may be described as having a $T_1OT_2\bar{T}_2\bar{O}T_1$ module (Table 6). Within the reyerite–gyrolite group, there is a spectrum of crystal-structure complexity, progressing from

fedorite with the simplest module (one T and one O layer, and no interlayer component), to gyrolite (Table 6). Minehillite, $[(K,Na)_2Ca_{28}Zn_5Al_4Si_{40}O_{112}(OH)_{16}$, space group $P\bar{3}c1$, with a 9.777 and c 33.293 Å; Dai *et al*. 1995] has a structure closely related to that of members of the reyerite–gyrolite group, but is not included therein. Whereas it possesses modules that are reminiscent of the $T_2\bar{T}_2$ double layers of tetrahedra, these double layers are in fact composed of pairs of inverted tetrahedra sharing common apices (Si–Al–Si) with AlO_6 octahedra, with an infinite layer being built up through edge-sharing with ZnO_4 tetrahedra (Bonaccorsi & Merlino 2005). Furthermore, although the crystal structure of orlymanite remains unknown, there is strong evidence that it is indeed related to those of other minerals of the reyerite–gyrolite group (Peacor *et al*. 1990) and hence, the mineral has been included. Using the terminology of Merlino (1988a), martinite can be described as having a $OT_2X\bar{T}_2O$ module. Although such a module is known in synthetic phases (*e.g.*, the Z-phase; Table 6), martinite represents the first mineral recognized to have it. Martinite is also unique in that it is the first member of the reyerite group found to contain essential boron.

Given the nature and magnitude of the crystal-structure variations possible in minerals of the reyerite–gyrolite group, this group does not strictly constitute a *polysomatic series* (Ferraris 1997). Rather, the presence of a basic reyerite-like module, with or without a variable interlayer component, suggests that the group represents a *merotype series,* and hence the term *reyerite–gyrolite merotype series* (Ferraris 1997) may be most appropriate when combining these minerals into one group based on crystal-structure similarities.

GENETIC IMPLICATIONS

Minerals of this reyerite–gyrolite group, which now includes martinite, are generally interpreted to be late-stage phases produced through low-T hydrothermal alteration or metamorphism of mafic rocks (usually alkali basalts). They are most commonly found in vugs in assemblages that include other hydrous low-T minerals (*e.g.*, zeolites). Owing to the significance of phases present in, and related to, the reyerite–gyrolite group in the cement industry (Taylor 1997) and in the development of radioactive waste repositories (Carroll *et al*. 1998), a large number of studies involving the syntheses of these minerals has been conducted. These have shown that for calcium silicate hydrate (*C–S–H*) members of the reyerite group, only a poorly ordered *C–S–H* gel exists below 120°C, between 140 and 240°C either the poorly defined Z-phase (Assarsson 1957) or gyrolite is stable, and above 200°C, truscottite is stable. Shaw *et al*. (2002) demonstrated that in the above system over the range 190 to 240°C, the formation of gyrolite involves a three-step process of crystallization:

amorphous gel → *C–S–H* gel → Z-phase → gyrolite. Further heating of gyrolite in the range of 400–600°C results in its conversion to a truscottite-like phase (*via* dehydration and polymerization of layers of tetrahedra). With continued heating, the truscottite-like phase degrades until 700°C, at which point only an amorphous material remains (Garbev *et al*. 2004). In the case of the Z-phase → gyrolite conversion, Shaw *et al*. (2002) opined that the process operates *via* a continuous, diffusion-controlled mechanism involving the ordering of the silicate layers and an increase in order along **c**. They also highlighted the fact that the Z-phase is likely to be unstable and transient (*i.e.*, metastable). The above results have important ramifications for the origin of martinite, as they demonstrate that minerals related to reyerite and martinite can be easily produced at T less than 250°C. Secondly, as the crystal structure of martinite most closely resembles that of the Z-phase, it suggests that martinite, like the Z-phase, may crystallize through the ordering of a precursor, gel-like material. Lastly, given the crystal-structure similarity of martinite and the Z-phase, the implication is that martinite, like the Z-phase, may effectively be metastable, although there is no evidence of decrepitation of martinite in the samples analyzed in this study.

REFERENCES

ASSARSSON, G.O. (1957): Hydrothermal reactions between calcium hydroxide and amorphous silica; the reactions between 180 and 220°. *J. Phys. Chem.* **61**, 474-479.

BONACCORSI, E. & MERLINO, S. (2005): Modular microporous minerals: cancrinite–davyne group and C–S–H phases. *In* Micro- and Mesoporous Mineral Phases (G. Ferraris & S. Merlino, eds.). *Rev. Mineral. Geochem.* **57**, 241-290.

BRESE, N.E. & O'KEEFFE, M. (1991): Bond-valence parameters for solids. *Acta Crystallogr.* **B47**, 192-197.

CARROLL, S.A., ALAI, M. & BRUTON, C.J. (1998): Experimental investigation of cement, Topopah Spring tuff, and water interactions at 200°C. *Appl. Geochem.* **13**, 571-579.

CHAO, G.Y. & ERCIT, T.S. (1991): Nalipoite, sodium dilithium phosphate, a new mineral species from Mont Saint-Hilaire, Quebec. *Can. Mineral.* **29**, 565-568.

CROMER, D.T. & LIBERMAN, D. (1970): Relativistic calculation of anomalous scattering factors for X rays. *J. Chem. Phys.* **53**, 1891-1898.

CROMER, D.T. & MANN, J.B. (1968): X-ray scattering factors computed from numerical Hartree–Fock wave functions. *Acta Crystallogr.* **A24**, 321-324.

DAI, YONGSHAN, POST, J.E. & APPLEMAN, D.E. (1995): Crystal structure of minehillite: twinning and structural relationships to reyerite. *Am. Mineral.* **80**, 173-178.

FARMER, V.C. (1974): *The Infrared Spectra of Minerals*. The Mineralogical Society, London, U.K.

FERRARIS, G. (1997): Polysomatism as a tool for correlating properties and structure. *In* Modular Aspects of Minerals (S. Merlino, ed.). *Eur. Mineral. Union, Notes in Mineral.* **1**, 275-295.

FERRARIS, G., PAVESE, A. & SOBOLEVA, S.V. (1995): Tungusite: new data, relationship with gyrolite and structural model. *Mineral. Mag.* **59**, 535-543.

GABE, E.J., LE PAGE, Y., CHARLAND, J.-P., LEE, F.L. & WHITE, P.S. (1989): NRCVAX – an interactive program system for structural analysis. *J. Appl. Crystallogr.* **22**, 384-387.

GARBEV, K., BLACK, L., STUMM, A., STEMMERMANN, P. & BASHAROVA, B. (2004): Polymerization reactions by thermal treatment of gyrolite-group minerals – an IR spectroscopic and X-ray diffraction study based on synchrotron radiation. *In* Proc. 8th Int. Congress on Applied Mineralogy, (M. Pecchio, F.R.D. Andrade, L.Z. D'Agostino, H. Kahn, L.M. Sant'Agostino and M.M.M.L. Tassinari, eds.). *International Council for Applied Mineralogy do Brasil* (ICAM–BR), 245-248.

GARD, J.A., LUKE, K. & TAYLOR, H.F.W. (1981): The crystal structure of K-phase. *Kristallografia* **26**, 1218-1223.

GARD, J.A., MITSUDA, T. & TAYLOR, H.F.W. (1975): Some observations on Assarson's Z-phase and its structural relations to gyrolite, truscottite, and reyerite. *Mineral. Mag.* **40**, 325-334.

GRICE, J.D. & GAULT, R.A. (1998): Thomasclarkite-(Y), a new sodium – rare-earth-element bicarbonate mineral species from Mont Saint-Hilaire, Quebec. *Can. Mineral.* **36**, 1293-1300.

GUGGENHEIM, S. & EGGLETON, R.A. (1987): Modulated 2:1 layer silicates: review, systematics and predictions. *Am. Mineral.* **72**, 724-738.

HORVÁTH, L. & PFENNINGER, E. (2000): I minerali di Mont Saint-Hilaire. *Riv. Mineral. Ital.* **3**, 140-204.

LACHOWSKI, E.E., MURRAY, L.W. & TAYLOR, H.F.W. (1979): Truscottite: composition and ionic substitutions. *Mineral. Mag.* **43**, 333-336.

MANDARINO, J.A. (1981): The Gladstone–Dale relationship. IV. The compatibility concept and its application. *Can. Mineral.* **19**, 441-450.

MERLINO, S. (1988a): Gyrolite: its crystal structure and crystal chemistry. *Mineral. Mag.* **52**, 377-387.

MERLINO, S. (1988b): The structure of reyerite, $(Na,K)_2Ca_{14}Si_{22}Al_2O_{58}(OH)_8 \cdot 8H_2O$. *Mineral. Mag.* **52**, 247-257.

MITCHELL, R.H. & BURNS, P.C. (2001): The structure of fedorite: a re-appraisal. *Can. Mineral.* **39**, 769-777.

NOLZE, G. & KRAUS, W. (1998): POWDERCELL, v. 2.3. Federal Institute for Materials Research and Testing, Berlin, Germany.

PEACOR, D.R., DUNN, P.J. & NELEN, J.A. (1990): Orlymanite, $Ca_4Mn_3Si_8O_{20}(OH)_6 \cdot 2H_2O$, a new mineral from South Africa: a link between gyrolite-family and conventional phyllosilicate minerals? *Am. Mineral.* **75**, 923-927.

SHAW, S.M., HENDERSON, C.M.B. & CLARK, S.M. (2002): In-situ synchrotron study of the kinetics, thermodynamics, and reaction mechanisms of the hydrothermal crystallization of gyrolite, $Ca_{16}Si_{24}O_{60}(OH)_8 \cdot 14H_2O$. *Am. Mineral.* **87**, 533-541.

SHELDRICK, G.M. (1993): SHELXL–93: a Program for the Refinement of Crystal Structures. Univ. of Göttingen, Göttingen, Germany.

TAYLOR, H.F.W. (1997): *Cement Chemistry*. Academic Press, San Diego, California.

VAN VELTHUIZEN, J. (1990): A hornfels unit in the Poudrette quarry. *Mineral. Rec.* **21**, 360-362.